

Magnetic resonance and ultrasound image-guided navigation system using a needle manipulator.

著者	YAMADA Atsushi, Tokuda Junichi, NAKA Shigeyuki, MURAKAMI Koichiro, TANI Tohru, MORIKAWA Shigehiro
journal or publication title	Medical physics
year	2019-12-12
URL	http://hdl.handle.net/10422/00012618

doi: 10.1002/mp.13958(<https://doi.org/10.1002/mp.13958>)

1 **Magnetic resonance and ultrasound image-guided navigation system using a needle**
2 **manipulator**

3
4 **Short running title:** Multi-modal image-guided navigation
5

6 Atsushi Yamada, PhD ¹⁾, Junichi Tokuda, PhD ²⁾, Shigeyuki Naka, MD PhD ³⁾, Koichiro
7 Murakami, MD, PhD ³⁾, Tohru Tani, MD PhD ¹⁾, Shigehiro Morikawa, MD PhD ⁴⁾

- 8
9 1) *Department of Research and Development for Innovative Medical Devices and*
10 *Systems, Shiga University of Medical Science, Seta Tsukinowa-cho, Otsu, Shiga 520-*
11 *2192, Japan*
12 2) *National Center for Image Guided Therapy, Brigham and Women's Hospital and*
13 *Harvard Medical School, Boston, Massachusetts 02115, USA*
14 3) *Department of Surgery, Shiga University of Medical Science, Seta Tsukinowa-cho,*
15 *Otsu, Shiga, 520-2192, Japan*
16 4) *Molecular Neuroscience Research Center, Shiga University of Medical Science, Seta*
17 *Tsukinowa-cho, Otsu, Shiga 520-2192, Japan*
18

19 **Corresponding author:**

20 Atsushi Yamada, PhD
21 *Department of Research and Development for Innovative Medical Devices and Systems,*
22 *Shiga University of Medical Science, Seta Tsukinowa-cho, Otsu, Shiga 520-2192, Japan*
23 Tel: +81-77-548-2345, Fax: +81-77-548-2132
24 E-mail: ayamada@belle.shiga-med.ac.jp
25

26 **ABSTRACT**

27 **Purpose:** Image guidance is crucial for percutaneous tumor ablations, enabling accurate
28 needle-like applicator placement into target tumors while avoiding tissues that are sensitive
29 to injury and/or correcting needle deflection. Although ultrasound (US) is widely used for
30 image guidance, magnetic resonance (MR) is preferable due to its superior soft tissue
31 contrast. The objective of this study was to develop and evaluate an MR and US multi-modal
32 image-guided navigation system with a needle manipulator to enable US-guided applicator
33 placement during MRI-guided percutaneous tumor ablation.

34 **Methods:** The MRI-compatible needle manipulator with US probe was installed adjacent to
35 a 3 Tesla MRI scanner patient table. Coordinate systems for the MR image, patient table,
36 manipulator, and US probe were all registered using an optical tracking sensor. The patient
37 was initially scanned in the MRI scanner bore for planning and then moved outside the bore
38 for treatment. Needle insertion was guided by real-time US imaging fused with the
39 reformatted static MR image to enhance soft tissue contrast. Feasibility, targeting accuracy,
40 and MR compatibility of the system were evaluated using a bovine liver and agar phantoms.

41 **Results:** Targeting error for 50 needle insertions was 1.6 ± 0.6 mm (mean \pm standard
42 deviation). The experiment confirmed that fused MR and US images provided real-time
43 needle localization against static MR images with soft tissue contrast.

44 **Conclusions:** The proposed MR and US multi-modal image-guided navigation system using a
45 needle manipulator enabled accurate needle insertion by taking advantage of static MR and
46 real-time US images simultaneously. Real-time visualization helped determine needle depth,

47 tissue monitoring surrounding the needle path, target organ shifts, and needle deviation

48 from the path.

49 **Key words:** medical robot, magnetic resonance imaging, image-guided therapy, liver

50 ablation

51

52 1. INTRODUCTION

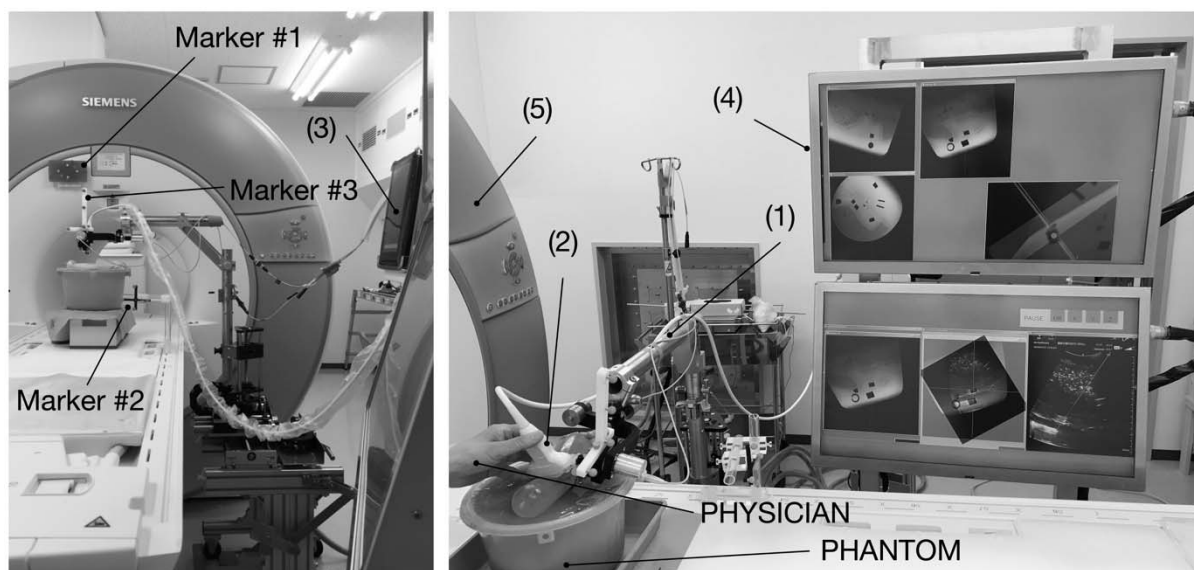
53 Percutaneous tumor ablations, such as ethanol injection, cryotherapy, laser interstitial
54 thermal therapy, radiofrequency ablation, and microwave coagulation therapy are widely
55 performed for patients who are not candidates for surgical resection¹⁻³. Those procedures
56 are often performed under image guidance to place needle-like applicators into target
57 tumors accurately while avoiding tissues that may be sensitive to injury and/or correcting
58 needle deflections. Image guidance is particularly important when a target organ is moving
59 due to respiration. Although ultrasonography and computed tomography (CT) are
60 commonly employed, intra-procedural magnetic resonance imaging (MRI) has also been
61 investigated^{4,5} due to its superior soft tissue contrast. One technical challenge for intra-
62 procedural MRI is to allow the physician to interactively maneuver the needle under real-
63 time image guidance because conventional closed-bore MRI inhibits the physician from
64 accessing the treated area.

65 We previously developed a real-time MRI-guided navigation system⁶⁻⁸ dedicated for a
66 0.5 Tesla (T) vertical open-configuration MRI scanner (Signa SP/2, GE Healthcare,
67 Milwaukee, WI)⁹. This navigation system leveraged the unique scanner configuration,
68 allowing physicians to access the patient in the bore during scanning, and hence enabling
69 interactive planning and targeting using a handheld needle guide^{10,11}. This system was
70 subsequently successfully employed for microwave ablations of liver tumors in more than
71 300 clinical cases from 2000 to 2016^{6-8,12-14}. We recently developed an MRI-compatible
72 cooperative needle manipulator¹⁵ to replace the handheld needle guide, providing more
73 interactive and accurate targeting, and successfully clinically tested this system for 23
74 ablation cases¹⁶. The study demonstrated that the physical assistance provided by the

75 cooperative needle manipulator improved targeting interactivity under MRI guidance and
76 helped reduce trial-and-error attempts before reaching the target. However, the
77 manipulator is incompatible with conventional closed-bore MRI scanners because its
78 mechanical configuration and clinical workflow are highly dependent on the specific open-
79 configuration MRI scanner.

80 The goal of this study was to enable the physician to interactively maneuver a needle
81 under MRI guidance for percutaneous tumor ablation using a widely available closed-bore
82 MRI scanner. To achieve this, we developed a multi-modal image-guided navigation system
83 where needle placement occurs outside the MRI scanner under MRI–ultrasound (US) fusion
84 guidance combined with physical assistance provided by the needle manipulator. The
85 system adapted an “in/scan-out/adjust technique”¹⁷ where the patient was scanned in the
86 bore for planning and then moved out for needle placement and adjustment. The
87 manipulator was equipped with a US probe to provide real-time image feedback during
88 needle insertion. The navigation system could also visualize multiplanar reconstructed
89 (MPR) MR images with sections synchronized with the US image plane in real-time to help
90 localize the target lesion and surrounding anatomical structures. We evaluated MRI-
91 compatibility, targeting accuracy, and device setup duration for realistic clinical workflows,
92 and system and workflow feasibility were demonstrated for a bovine liver phantom.

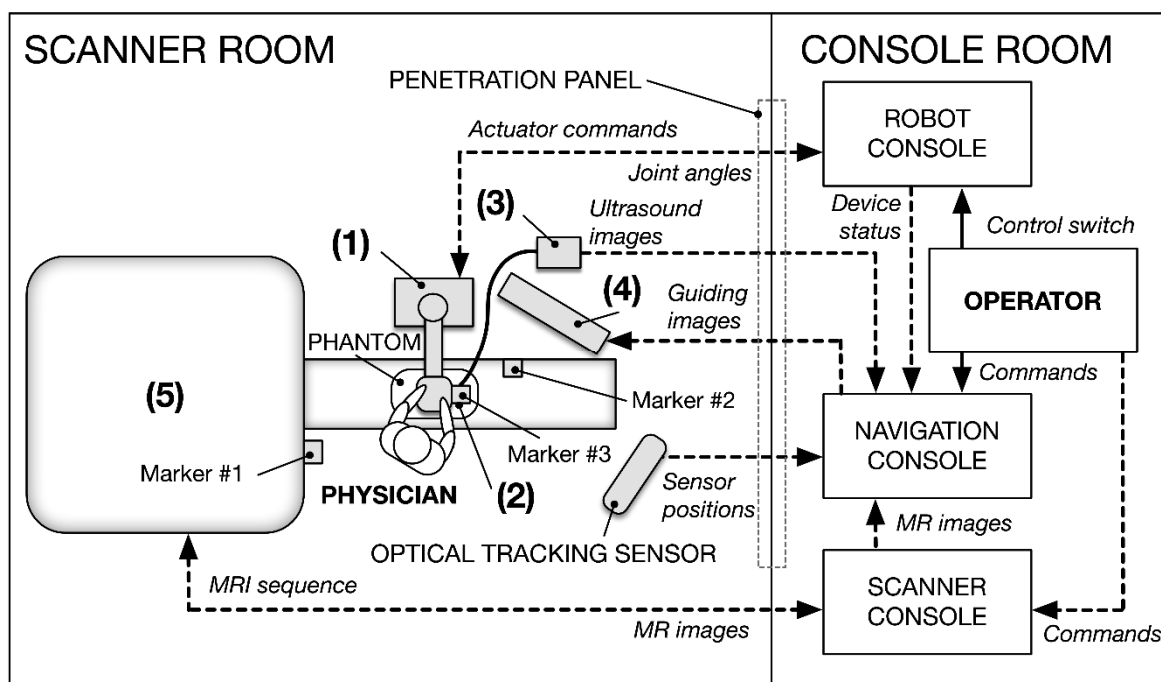
93



94

95 **FIG. 1.** Proposed navigation system based on simultaneous robotic and image guidance for
 96 interactive needle path planning and accurate needle placement: (1) needle manipulator;
 97 (2) ultrasound (US) probe; (3) US imaging scanner; (4) in-room monitors to display image
 98 guidance; (5) closed-bore MRI scanner; markers #1, #2, and #3 were used for the optical
 99 tracking sensor. A physician facing the needle manipulator across the patient table of the
 100 MRI scanner can interactively select an optimal needle path with the manipulator while
 101 observing the selected needle path candidate and surrounding structures (in this case for a
 102 phantom). Then, the physician can insert the needle along the needle guide while observing
 103 the insertion in US images with synchronized MR image plane on the monitors in real time.

104



105

106 **FIG. 2.** The proposed simultaneous robotic and image guidance system: Components (1)–(5)
107 are explained in Fig. 1. The system provides physician guidance in the scanner room with an
108 operator in the console room next to the scanner room. The phantom in this diagram
109 represents a patient’s abdomen.

110

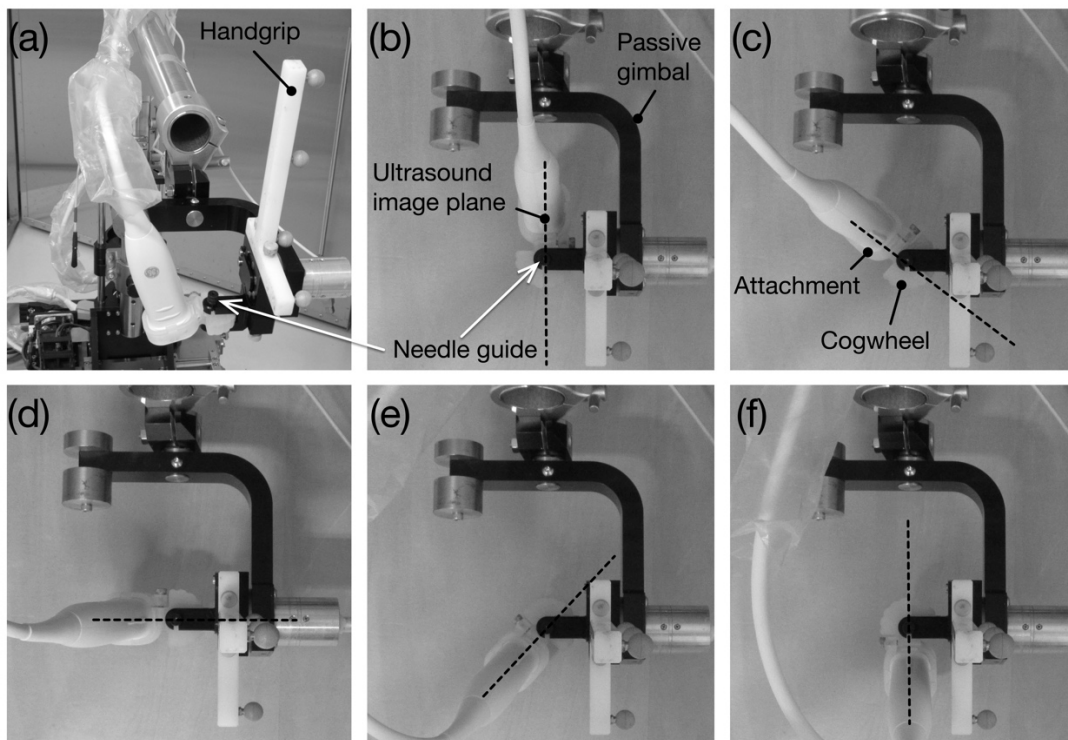
111 **2. MATERIALS AND METHODS**

112 **2.A. System overview**

113 The developed navigation system comprised a needle manipulator with US probe, in-room
114 monitors, optical tracking sensor, and wide-bore 3 T MRI scanner (Magnetom Verio 3T,
115 Siemens Healthcare, Erlangen, Germany) (Figs. 1 and 2). The hardware components were all
116 placed in the scanner room and connected to robot and navigation consoles in the console
117 room through a radio frequency filtered penetration panel (Riken Electromagnetic
118 Compatibility Inc., Fukuoka, Japan) with waveguides. Customized image guidance software
119 was installed on the navigation console.

120 **Ultrasound imaging scanner.** A portable diagnostic US imaging scanner (Venue 40, GE
121 Healthcare) was integrated into the system to provide real-time image feedback during
122 needle insertion. Sector (3S-SC, GE Healthcare) or convex (4C-SC) probe can be selected
123 depending on the subject, and attached to the needle manipulator with 1.9 m cable. The US
124 imaging scanner frame was replaced with a non-ferromagnetic frame (aluminum) to
125 improve MRI safety.

126



127

128 **FIG. 3.** Needle manipulator passive end effector: (a) overview, and (b)–(f) top views. The
 129 installed ultrasound (US) probe could be rotated 180° around the needle guide positioned at
 130 the intersection of the two passive gimbal rotational axes. The passive gimbal provided
 131 sufficient space for the US probe to be rotated. White solid arrows represent needle guide
 132 locations and dotted lines represent the US imaging plane.

133

134 **Needle manipulator.** The manipulator was a portable robotic arm comprising an end
 135 effector with passive gimbal and three-axis active linear base stage mounted on a four-
 136 wheel cart, where the linear base stage and cart were adapted from our previous works^{15,16}.
 137 The range of motion for the linear base stage driven by non-magnetic ultrasonic motors was
 138 230, 185, and 150 mm (width, depth, and height, respectively). The end effector was fixed
 139 to an L-shaped rigid arm mounted on the vertical axis of the linear base stage such that it
 140 was positioned above the patient table. The end effector comprised a needle guide and
 141 handgrip mounted on a two degrees of freedom (DOF) passive gimbal (Fig. 3). Each passive
 142 joint on the gimbal had a nonmagnetic optical rotary encoder (Prototype, Oshima Prototype

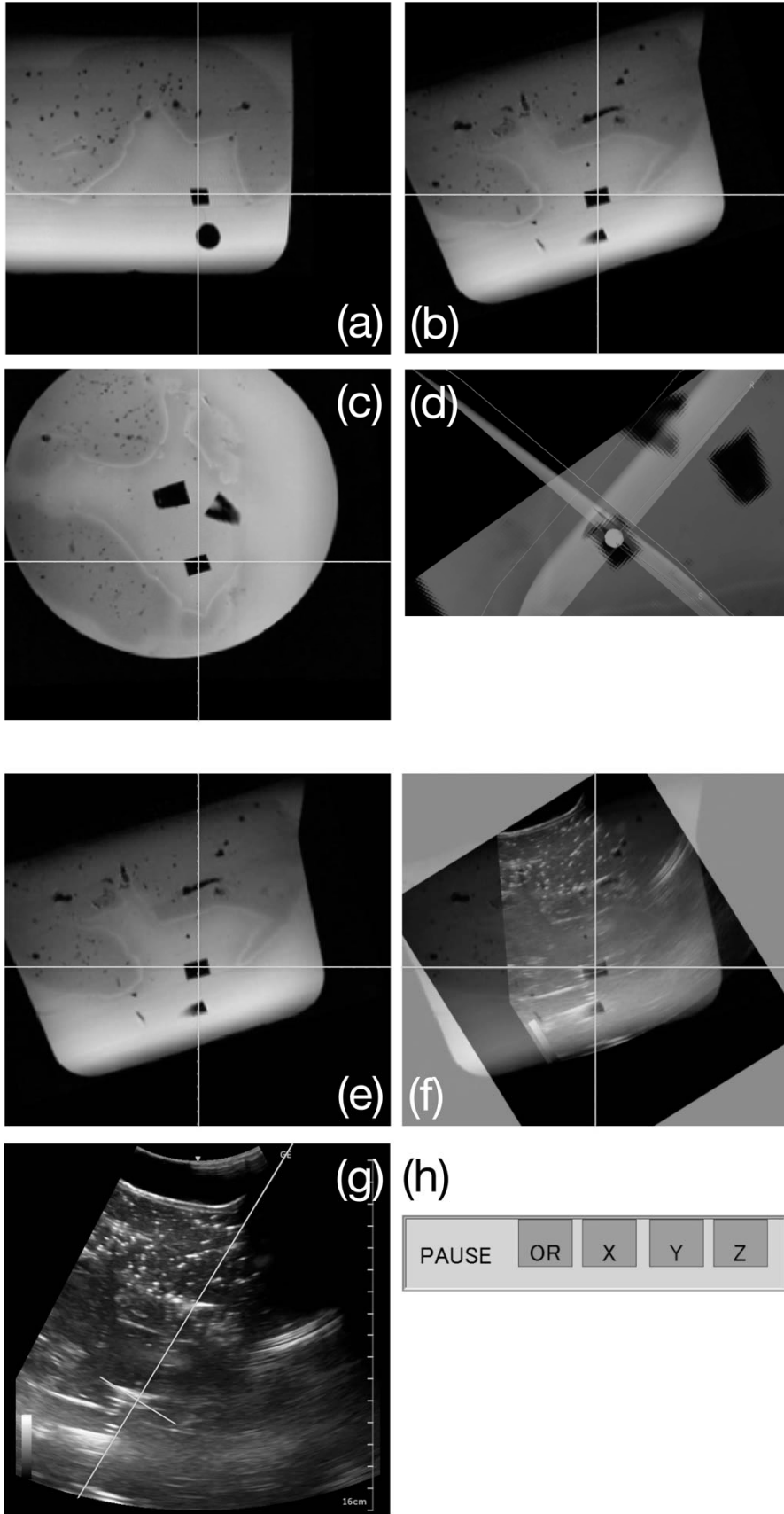
143 Engineering, Tokyo, Japan) to detect rotational angle. The needle path intersected the
144 crossing point of the two rotational axes. The needle guide included an unlock mechanism
145 with rotational collet to detach the inserted needle from the end effector. The US probe was
146 attached to the needle guide via a concentric cogwheel to facilitate adjusting the US scan
147 plane angle with respect to the needle path (Fig. 3). The US scan plane always coincided
148 with the needle insertion plane and the cogwheel could be rotated at 22.5° intervals. The US
149 probe could be detached from the needle guide.

150 The manipulator allowed a physician to tilt the needle guide freely via the handgrip¹⁸
151 while the base stage automatically adjusted the needle guide position using virtual remote
152 center of motion (Virtual RCM) control¹⁹ to maintain the preset distance between the
153 needle guide and target, and keep the needle directed at the target, as shown elsewhere¹⁵.
154 The ultrasonic motors and encoders can be turned on or off at the robot console
155 workstation, which also sends device status to the navigation console.

156 **Tracking sensor.** An optical tracking sensor (a Polaris Spectra position sensor with Extended
157 Pyramid Volume (EPV)²⁰, Northern Digital Inc., Ontario, Canada) was used to register the
158 MRI scanner, scanner patient table, and needle guide coordinate systems. Coordinate
159 registration was crucial, since the table and needle manipulator were not permanently fixed
160 to the MRI scanner. The tracking sensor was mounted on a 130 cm high four-wheeled cart.
161 Passive marker units for the sensor were attached to the MRI scanner housing (marker #1),
162 patient table (marker #2), and needle guide (marker #3) (Figs. 1 and 2) to provide locations
163 in the sensor coordinate system. The frame for marker #3 was the handgrip of the passive
164 end effector. The tracking sensor sends continuous data to the navigation console.

165 **In-room monitors.** MRI-compatible in-room monitors (Prototype, Takashima Seisakusho,
166 Tokyo, Japan) displayed the image guidance graphical user interface (Fig. 4). The in-room
167 monitors were flat-panel displays arranged vertically. The upper monitor displayed planning
168 information, including three orthogonal MPR images perpendicular (transverse) and parallel
169 (in-plane-0 and in-plane-90) to the needle path and a virtual bird's eye view of the three
170 MPR image planes with a model of the target in the patient. The lower monitor displayed
171 guidance information, including real-time US image, corresponding MPR image, and their
172 fusion. The planned needle path was superimposed on the US image so the physician could
173 monitor needle deviations from the planned path in real-time. Device status, including
174 Virtual RCM mode status (on or off) and motion limit alerts for the three axis active linear
175 base stage were also displayed.

176

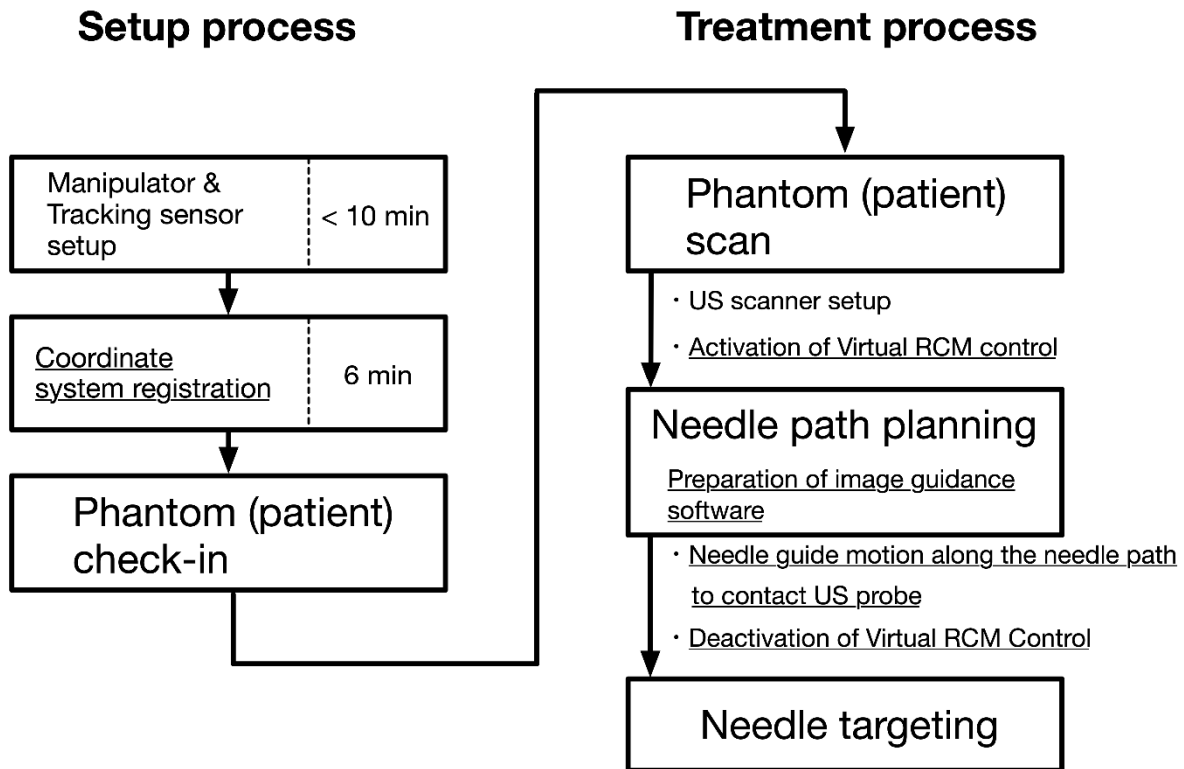


178 **FIG. 4.** Typical guiding images displayed on the (a)–(d) upper and (e)–(h) lower in-room
179 monitors: (a) in-plane-0 multiplanar reconstruction (MPR) parallel to the needle path),
180 where the vertical line represents the planned needle path, and its intersection with the
181 solid horizontal line represents the target location; (b) in-plane-90 MPR; (c) MPR
182 perpendicular to the needle path; (d) virtual bird's eye view; (e) corresponding MPR (in-
183 plane-90 image in this figure; (f) ultrasound (US) image plane fused with the in-plane-90
184 image; (g) US image plane, where the long solid line represents the planned needle path,
185 and the intersection with the short solid line represents the target location; (h) device
186 status, i.e., (left to right) virtual remote center of motion mode status and motion limit
187 alerts for the three axis active linear base stage.

188

189 **Image guidance software.** The image guidance software worked as an information hub for
190 the entire system and provided following features: importing images from the MRI and US
191 scanners, position and orientation of markers from the tracking sensor, and device status
192 from the robot console, and visualizing them effectively with the procedure plan on the in-
193 room monitors to navigate the procedure. Once the coordinate systems described above
194 (*Tracking sensor*) were registered, the software could generate MPR images from MR
195 images that were parallel and perpendicular to the US imaging plane. The software was
196 developed in-house in C++ (Visual Studio 2008, Microsoft Corp., Redmond, WA) and
197 installed on a navigation console workstation (Z800, 2.26 GHz dual quad-core Intel Xeon
198 E5520 Processors, 24 GB 1,333 MHz DDR3 ECC RAM, NVIDIA Quadro FX 3800, HP Inc., Palo
199 Alto, CA) with the Windows operating system (Windows 7 Professional 64-bit Service Pack 1,
200 Microsoft Corp.). Ultrasound images were captured continuously by an image signal
201 converter (DVI2USB 3.0, Epiphan Systems, Ottawa, Canada) and imported into the software
202 using a free open-source computer vision library (OpenCV 2.4.10, Intel Corporation, Santa
203 Clara, CA).

204



205

206 **FIG. 5.** Needle placement workflow using the proposed multi-modal image-guided
 207 navigation system with needle manipulator. The setup process includes duration for each
 208 phase, and tasks for the system operator in the console room are underlined.

209

210 2.B. Workflow

211 The workflow was designed based on our previous work¹⁶ and included three phases in both
 212 the setup and treatment processes, as shown in Fig. 5, including indicative setup component
 213 durations. In the manipulator and tracking sensor setup phase, the manipulator was placed
 214 next to the patient table without attaching the US probe. The actuator power supply cables
 215 and the optical fiber cables of the encoders were connected to the robot console through
 216 the waveguide on the penetration panel. A tracking sensor was located in the scanner room
 217 such that all three markers were in the measurement volume. Registration with manipulator
 218 calibration was performed by the operator, the registration transformation matrix was

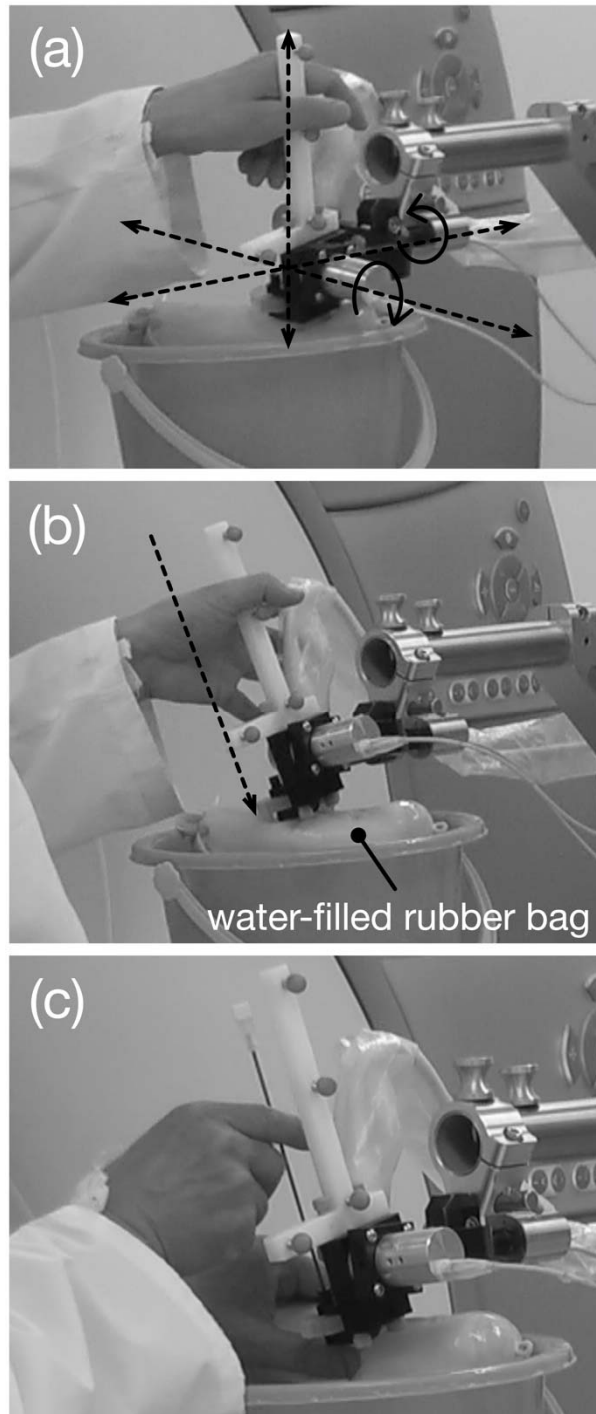
219 loaded into the image guidance software, and then a phantom (patient) was placed on the
220 table. The manipulator motor and encoder power supplies were turned off after setup
221 completed.

222 The planning image was acquired in the scan phase. The US probe was not present in
223 the MRI room during scanning to avoid electromagnetic (EM) interference with MRI. The
224 patient table was then moved to the manipulator workspace. Targets were identified
225 visually in the MR images on the scanner console, their coordinates were recorded, and the
226 planning image was loaded into the image guidance software. One of the target coordinates
227 was manually entered into the robot console, the motors and encoders were turned on, and
228 the US probe was attached to the end effector, requiring less than one minute.

229 The manipulator was used for both path planning and needle targeting phases (Fig. 6).
230 In the planning phase, the operator first set the preset distance on the image guidance
231 software and then Virtual RCM control was activated. The physician stood on the lateral side
232 of the patient table facing the manipulator and selected the optimal needle path by tilting
233 the passive gimbal while observing guidance images on the upper monitor (Fig. 4). The
234 needle guide was then moved along the selected needle path with the US probe making
235 contact with the phantom (patient) surface through a water-filled rubber bag.

236 Virtual RCM control was turned off during the targeting phase to avoid unexpected
237 actuation if the gimbal was accidentally rotated by contact with the phantom surface
238 (patient's body). The physician then inserted the needle manually along the needle guide
239 while observing the guidance images on the lower monitor (Fig. 4). The operator managed
240 manipulator phase transitions on the robot console workstation, as shown in Fig. 5.

241



242

243 **FIG. 6.** Needle manipulator end effector in the interactive needle path planning and
 244 targeting phases: (a) end effector manipulation in the planning phase, solid arrows
 245 represent rotational motions by the physician facing the manipulator and dotted arrows
 246 represent translational directions of the needle manipulator three axis active linear base
 247 stage; (b) needle guide motion along the needle path to place the ultrasound probe in

248 contact with the water-filled rubber bag on the phantom; and (c) end effector in the
249 targeting phase, the physician inserts the needle along the needle guide.

250

251 **2.C. Feasibility using a phantom**

252 A mock procedure was performed with a phantom to qualitatively evaluate the proposed
253 navigation system and its workflow. The phantom was a 2.5 kg bovine liver submerged in
254 2% agar (010-15815 agar powder, Wako Pure Chemical Industries, Ltd., Osaka, Japan) mixed
255 with 0.25 mM Gd-DTPA in a plastic container, with small pieces of acrylic rods and tubes
256 distributed randomly as targets. A convex probe was used for US imaging. The scan phase
257 acquired a T1 weighted 3D image in the coronal plane with a Spine Matrix Coil using a 3D
258 fast acquisition low flip angle spoiled gradient echo sequence (TR/TE = 8.6/3.86 ms; flip
259 angle = 25°; acquisition matrix = 256×256; field of view (FOV) = 240×240 mm²; slice
260 thickness = 2.5 mm). The preset distance was set to 150 mm to avoid contact between the
261 needle guide and phantom surface during path planning. After path planning, the water-
262 filled rubber bag was placed on the phantom surface with the appropriate amount of gel
263 (Aquasonic 100 Ultrasound Transmission Gel, 250 ml, Parker Laboratories, Inc., Fairfield, NJ)
264 (Fig. 6). The needle guide was moved along the needle path until the US probe had sufficient
265 contact with the rubber bag, and then a 20 cm 14 gauge MRI-compatible needle (Invivo,
266 Gainesville, FL) with a beveled tip was used. We performed the feasibility study five times
267 and recorded the time required for each setup (Fig. 5).

268 **2.D. Assessment of needle placement accuracy**

269 The targeting accuracy was assessed using an agar phantom made of 2% agar mixed with
270 0.25 mM Gd-DTPA in a plastic container. After scanning using the same imaging protocol
271 described above, we set the centroids of ten targets in the depth range 30–80 mm. We
272 designed five needle paths including a vertical path and four oblique paths for each target
273 by tilting the needle guide in a range of about $\pm 25^\circ$. The preset distance was set to 150 mm.
274 The needle was inserted using the needle guide while rotating the needle about its axis to
275 avoid needle deviation from the planned path. After insertion, the needle was retracted
276 while suctioning the agar on the needle path with a syringe attached to the needle top to
277 ensure the needle path was visible on the confirmation MR image. We performed 50 needle
278 targeting exercises for all ten targets. After targeting was completed, a confirmation image
279 was acquired using the same protocol as the planning image.

280 The confirmation image was assessed using 3D Slicer software²¹ to measure the
281 distance between the needle path location and the target centroid orthogonal to the needle
282 path. In-plane distances for all paths were recorded as targeting errors and their average
283 and standard deviations were calculated.

284 **2.E. Impact on MR images**

285 We measured the signal to noise ratio (SNR) and distortion on MR images to assess the
286 proposed system impact. Six incremental system configurations were considered:

287 (1) Baseline: only the phantom and monitors were placed in the scanner room;

- 288 (2) Manipulator in Place: the manipulator and tracking sensor were placed in the
289 scanner room but not connected to the robot console;
- 290 (3) Cable in Place: the cables were placed through the waveguide but not connected to
291 the console;
- 292 (4) Cable Connected: the manipulator and tracking sensor were connected to the robot
293 console;
- 294 (5) Manipulator Ready: the manipulator and tracking sensor were switched on; and
- 295 (6) System Ready: the US scanner was installed into the manipulator and connected to
296 the navigation console.

297 We scanned an agar phantom for these assessments using two MRI pulse sequences:
298 two-dimensional turbo spin echo (2D TSE) (TR/TE = 4,060/13 ms, acquisition matrix =
299 256×256; FOV = 150×150 mm²; slice thickness = 5 mm; number of slices = 16), and three-
300 dimensional gradient echo (3D GRE) (TR/TE = 60/8 ms; flip angle = 45°; acquisition matrix =
301 256×256; FOV = 150×150 mm², slice thickness = 5 mm; number of slices = 24). We used the
302 difference image method for SNR measurement^{22,23} and evaluated distortion by measuring
303 phantom diameter on the image for each configuration.

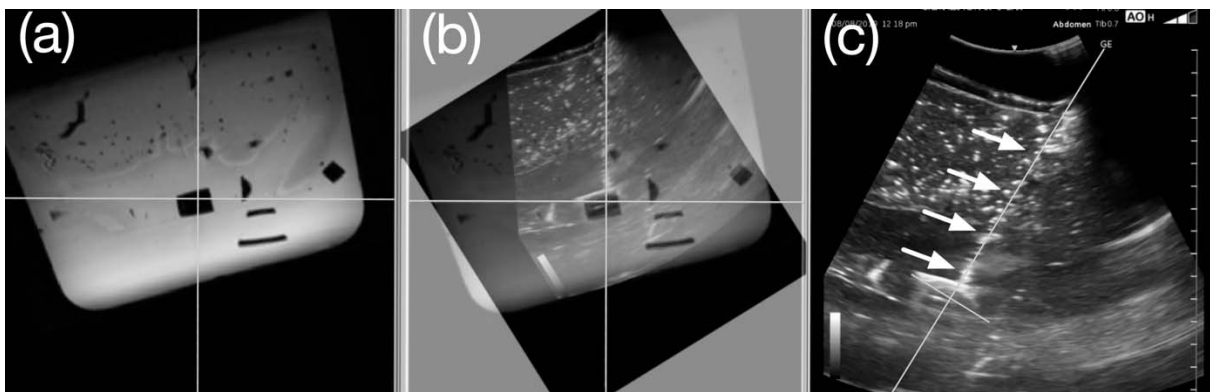
304 **3. RESULTS**

305 **3.A. Feasibility**

306 The mock procedure was completed successfully. Figure 7 shows highlighted screenshots
307 from the image guidance software displaying the needle. We visually confirmed that real-
308 time US images visualized the needle path plane including the target, needle on the planned
309 path, and surrounding soft tissue structures of the bovine liver. Alignment between the

310 planning MR and US images was visually assessed by observing the superimposed target and
 311 adjacent object outlines. Needle tip placement at the target was also confirmed on both
 312 images. Average times for manipulator and tracking sensor setup, coordinate system
 313 registration, and US scanner setup were 9.4 min, 5.7 min, and 51.4 s, respectively.

314



315

316 **FIG. 7.** Typical guiding image screenshots: (a) in-plane-90 planning MRI image, where the
 317 solid vertical line represents the planned needle path, and its intersection with the solid
 318 horizontal line represents the target location; (b) ultrasound (US) image plane fused with in-
 319 plane-90 image; (c) US image plane with inserted needle, where the long solid line
 320 represents the planned needle path, the intersection with the short solid line represents the
 321 target location, and solid arrows indicate the inserted needle.

322

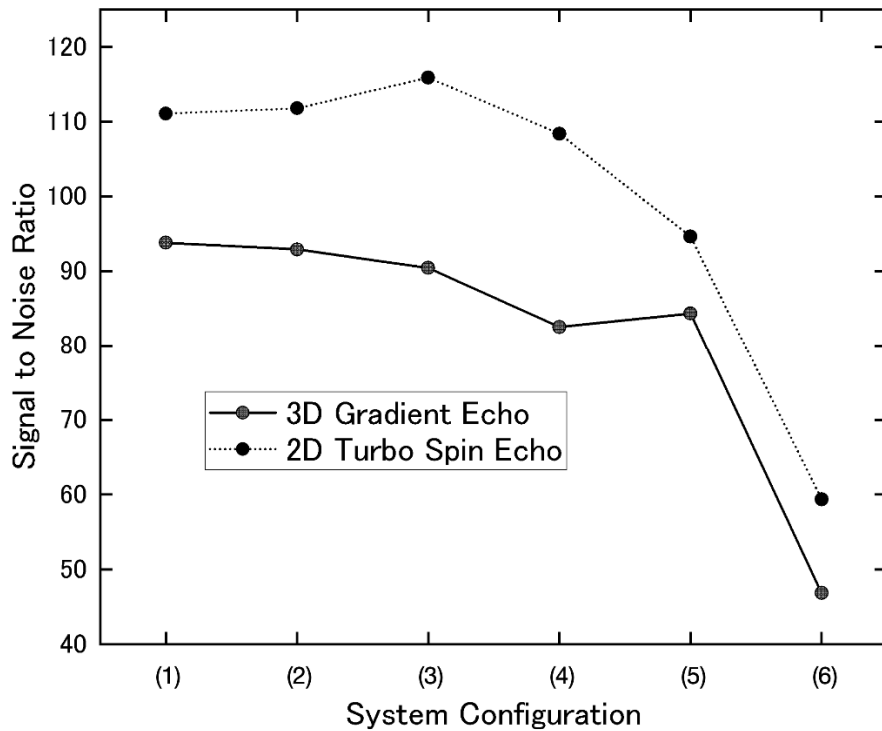
323 **3.B. Needle placement accuracy**

324 Targeting error over fifty trials was 1.6 ± 0.6 mm (mean \pm standard deviation), with
 325 maximum and minimum errors of 3.1 and 0.6 mm, respectively. Maximum and minimum
 326 needle path angles from the vertical line were 27.2° and -26.1° , respectively.

327 **3.C. Impact on MR images**

328 Figure 8 shows SNR for each configuration. SNR for 3D GRE was 46.9 for configuration 6 (see
329 Section 2.E), which was the lowest SNR among all conditions; whereas SNR for 3D GRE was
330 82.5 for configuration 4, which was used for the planning image scan (Fig. 5). Distortion
331 changes could not be confirmed in either sequence.

332



333

334 **FIG. 8.** Signal to noise ratio (SNR) for the system configurations detailed in Section 2.E.

335

336 4. DISCUSSION

337 We developed a multi-modal image-guided navigation system using a robotic needle
338 manipulator. Cooperative physician–device interaction with MRI guidance helped the
339 physician to follow the optimal needle path by fine tuning needle guide angles intuitively on
340 the MRI scanner patient table. The proposed system also provided real-time fusion images
341 on in-room displays after starting the needle targeting phase to help the physician confirm
342 safe and accurate needle insertion, enabling needle placement with sufficient accuracy for
343 liver tumor ablations¹¹. Coordinate registration was completed before the phantom
344 (patient) was placed on the table and hence did not disrupt treatment.

345 Several robotic assistance devices have been recently proposed for MRI-guided needle
346 insertion applications^{24,25}, including patient^{26–28} and scanner table^{29,30} mounted robotic
347 devices. Although patient mounted devices can be easily set up due to their small
348 footprints, they must be placed at the correct incision site on the patient prior to the
349 procedure, which may require repeated scanning and adjustments, prolonging procedure
350 time since the patient must be moved in and out of the MRI scanner bore for each
351 adjustment. However, the proposed method does not require this repeated process
352 because the manipulator can adjust the entry point with translational DOFs in contrast with
353 patient mounted devices. One limitation for the current proposed system is that the US
354 probe was not specifically designed for use in MRI scanner rooms, and must be removed
355 from the scanner room while the patient is being MRI scanned to ensure optimal MRI SNR
356 (Fig. 8). However, clinical workflow disruption to attach or detach the US scanner was
357 minimal, requiring approximately one minute.

358 Most MRI-guided needle insertion systems require confirmation MRI scan(s)³¹ to
359 determine insertion depth as the systems rely on low-resolution depth gauge²⁹ or scale on
360 the inserted needle. However, the proposed system monitors needle insertion with real-
361 time US imaging, synchronized MPR images, and the fused image helps determine needle
362 depth, monitor tissues surrounding the needle path, and identify target organ shifts and
363 needle deviations in real time.

364 Fusion image guidance combining MRI or CT with US imaging has been used clinically³²,
365 including EM needle tracking for liver lesions^{33–35}. Conventional US and contrast enhanced
366 MRI image fusion improves liver lesion visibility, which would otherwise be invisible on
367 conventional US images³⁶. Image fusion using EM tracking requires plane and point
368 registration to align MR and US images based on either external fiducial markers or internal
369 anatomical landmarks. However, achieving acceptable accuracy matching these points or
370 planes requires considerable training and experience³⁷. Previous studies showed average
371 registration error³⁸ of approximately 8 mm with best accuracy³⁹ of 1.9 ± 1.4 mm when US
372 images were obtained immediately after CT acquisition under anesthesia³². The proposed
373 navigation system and workflow eliminated training and experience requirements to
374 achieve acceptable accuracy because MRI and US imaging coordinate systems are managed
375 throughout the procedure by a single tracking sensor and markers attached to imaging
376 scanners.

377 The proposed system leverages cooperative physician–device interaction to enable the
378 physician to adjust needle guide angles directly in the scanner room. This physical input is
379 more intuitive than control through a graphical user interface because the physician can
380 maneuver the needle guide directly, without being distracted by needing to keep the needle

381 aligned with the target^{8,40}. Adjusting the needle guide contact surface to obtain better US
382 imaging is also very simple using the cogwheel.

383 Targeting error was equivalent to the authors' previous study using an open-
384 configuration MRI scanner¹⁵ even though the present system requires patient table motion
385 in the workflow. Thus, the proposed system would provide sufficient needle placement
386 accuracy for liver tumor ablation¹¹. Real-time needle location feedback through US and
387 fused images also allows the physician to immediately compensate for needle deviations,
388 which are more likely when operating *in vivo*.

389 The water-filled rubber bag between the US probe and phantom (patient) surface
390 ensures adequate contact between the probe and phantom surfaces, while allowing the
391 physician to freely access the entry point on the patient table outside the MRI scanner bore.
392 However, the rubber bag weight could risk potential surface (i.e., patient skin) deformation
393 in clinical environments. One potential solution to minimize surface deformation would be
394 to use commercially available sterile cover kits for the probe (CIV-Flex Covers, CIVCO
395 Medical Solutions, Coralville, IA), which covers the US probe with a soft and durable flexible
396 sheet for distortion-free imaging where the bottom part is filled with US transmission gel.
397 The sheet could be fixed in the proper position with a band. A US probe covered with such a
398 kit would enable adaptive contact between the probe and patient skin by deforming the
399 filled gel, while avoiding deformation due to gel weight.

400 This study was limited to phantoms, which, although useful to evaluate clinical
401 workflow feasibility, cannot incorporate several potentially confounding factors, such as
402 target organ shifts and physical interactions between the needle and actual tissue. Future

403 animal studies will help assess system accuracy in the presence of those factors and
404 potentially highlight the proposed system's advantages.

405 **5. CONCLUSIONS**

406 We developed an MRI and US multi-modal image-guided navigation system using a robotic
407 needle manipulator, and demonstrated accurate needle insertion and seamless phase
408 transitions were achievable with the proposed system.

409 **ACKNOWLEDGMENTS**

410 This work was supported by JSPS KAKENHI (grants 26282145 and 18H01408), and NIH
411 (grants R01EB020667 and P41EB015898).

412 **CONFLICT OF INTEREST STATEMENT**

413 J.T. receives funding from Siemens Medical Solutions USA Inc. for a research project
414 unrelated to the present study. The other authors have no COI to report.

415

416 REFERENCES

- 417 1. Poon RT, Fan ST, Tsang FH, Wong J. Locoregional therapies for hepatocellular
418 carcinoma: a critical review from the surgeon's perspective. *Ann Surg* 2002;
419 235(4):466–486.
- 420 2. Ido K, Isoda N, Sugano K. Microwave coagulation therapy for liver cancer :
421 laparoscopic microwave coagulation. *Gastroenterology* 2001; 36(3):145–152.
- 422 3. Head HW, Dodd GD, 3rd. Thermal ablation for hepatocellular carcinoma.
423 *Gastroenterology* 2004; 127(5 Suppl 1):S167–178.
- 424 4. Kahn T, Harth T, Kiwit JC, Schwarzmaier HJ, Wald C, Modder U. In vivo MRI
425 thermometry using a phase-sensitive sequence: preliminary experience during MRI-
426 guided laser-induced interstitial thermotherapy of brain tumors. *J Magn Reson*
427 *Imaging* 1998; 8(1):160–164.
- 428 5. Lewin JS, Connell CF, Duerk JL, et al. Interactive MRI-guided radiofrequency
429 interstitial thermal ablation of abdominal tumors: clinical trial for evaluation of
430 safety and feasibility. *J Magn Reson Imaging* 1998; 8(1):40–47.
- 431 6. Morikawa S, Inubushi T, Kurumi Y, et al. Advanced computer assistance for magnetic
432 resonance-guided microwave thermocoagulation of liver tumors. *Acad Radiol* 2003;
433 10(12):1442–1449.
- 434 7. Morikawa S, Inubushi T, Kurumi Y, et al. New assistive devices for MR-guided
435 microwave thermocoagulation of liver tumors. *Acad Radiol* 2003; 10(2):180–188.
- 436 8. Sato K, Morikawa S, Inubushi T, et al. Alternate biplanar MR navigation for
437 microwave ablation of liver tumors. *Magn Reson Med Sci* 2005; 4(2):89–94.
- 438 9. Schenck JF, Jolesz FA, Roemer PB, et al. Superconducting open-configuration MR
439 imaging system for image-guided therapy. *Radiology*. 1995; 195(3):805–814.
- 440 10. Silverman SG, Collick BD, Figueira MR, et al. Interactive MR-guided biopsy in an
441 open-configuration MR imaging system. *Radiology* 1995; 197(1):175–181.
- 442 11. Silverman SG, Tuncali K, Adams DF, et al. MR imaging-guided percutaneous
443 cryotherapy of liver tumors: initial experience. *Radiology* 2000; 217(3):657–664.
- 444 12. Shiomi H, Naka S, Sato K, et al. Thoracoscopy-assisted magnetic resonance guided
445 microwave coagulation therapy for hepatic tumors. *Am J Surg* 2008; 195(6):854–860.
- 446 13. Sonoda H, Shimizu T, Takebayashi K, et al. *Minimally invasive surgery using the open*
447 *magnetic resonance imaging system combined with video-assisted thoracoscopic*
448 *surgery for synchronous hepatic and pulmonary metastases from colorectal cancer:*
449 *report of four cases. Surg Today* 2015; 45(5):652–658.

- 450 14. Murakami K, Naka S, Shiomi H, et al. Initial experiences with MR Image-guided
451 laparoscopic microwave coagulation therapy for hepatic tumors. *Surg Today* 2015;
452 45(9):1173–1178.
- 453 15. Hata N, Tokuda J, Hurwitz S, Morikawa S. MRI-compatible manipulator with remote-
454 center-of-motion control. *J Magn Reson Imaging* 2008; 27(5):1130–1138.
- 455 16. Morikawa S, Naka S, Murakami K, et al. Preliminary clinical experiences of a
456 motorized manipulator for magnetic resonance image-guided microwave
457 coagulation therapy of liver tumors. *Am J Surg* 2009; 198(3):340–347.
- 458 17. Morrison PR, Silverman SG, Tuncali K, Tatli S. MRI-guided cryotherapy. *J Magn Reson*
459 *Imaging* 2008; 27(2):410–420.
- 460 18. Troccaz J, Delnondedieu Y. Semi-active guiding systems in surgery. A two-dof
461 prototype of the passive arm with dynamic constraints (PADyC). *Mechatronics* 1996;
462 6(4):399–421.
- 463 19. Boctor EM, Webster RJ, 3rd, Mathieu H, Okamura AM, Fichtinger G. Virtual remote
464 center of motion control for needle placement robots. *Comput Aided Surg* 2004;
465 9(5):175–183.
- 466 20. NDI Polaris position sensor. [https://www.ndigital.com/medical/products/polaris-](https://www.ndigital.com/medical/products/polaris-family/)
467 [family/](https://www.ndigital.com/medical/products/polaris-family/). Accessed January 22, 2019.
- 468 21. Fedorov A, Beichel R, Kalpathy-Cramer J, et al. 3D Slicer as an image computing
469 platform for the Quantitative Imaging Network. *Magn Reson Imaging* 2012;
470 30(9):1323–1341.
- 471 22. Murphy BW, Carson PL, Ellis JH, Zhang YT, Hyde RJ, Chenevert TL. Signal-to-noise
472 measures for magnetic resonance imagers. *Magn Reson Imaging* 1993; 11(3):425–
473 428.
- 474 23. Firbank MJ, Coulthard A, Harrison RM, Williams ED. A comparison of two methods
475 for measuring the signal to noise ratio on MR images. *Phys Med Biol* 1999;
476 44(12):N261–264.
- 477 24. Fisher T, Hamed A, Vartholomeos P, et al. Intraoperative magnetic resonance
478 imaging-conditional robotic devices for therapy and diagnosis. *Proceedings of the*
479 *Institution of Mechanical Engineers Part H, J Eng Med* 2014; 228(3):303–318.
- 480 25. Moche M, Zajonz D, Kahn T, Busse H. MRI-guided procedures in various regions of
481 the body using a robotic assistance system in a closed-bore scanner: preliminary
482 clinical experience and limitations. *J Magn Reson Imaging* 2010; 31(4):964–974.
- 483 26. Hata N, Song SE, Olubiyi O, et al. Body-mounted robotic instrument guide for image-
484 guided cryotherapy of renal cancer. *Med Phys* 2016; 43(2):843–853.

- 485 27. Wu F, Torabi M, Yamada A, et al. An MRI Coil-Mounted Multi-Probe Robotic
486 Positioner for Cryoablation. Paper presented at: 2013 ASME International Design
487 Engineering Technical Conferences & Computer and Information in Engineering
488 Conference IDETC/CIE; 4–7 Aug. 2013.
- 489 28. Song S, Tokuda J, Tuncali K, Yamada A, Torabi M, Hata N. Design evaluation of a
490 double ring RCM mechanism for robotic needle guidance in MRI-guided liver
491 interventions. Paper presented at: 2013 IEEE/RSJ International Conference on
492 Intelligent Robots and Systems; 3–7 Nov. 2013.
- 493 29. Franco E, Ristic M, Rea M, Gedroyc WM. Robot-assistant for MRI-guided liver
494 ablation: A pilot study. *Med Phys* 2016; 43(10):5347.
- 495 30. Stoianovici D, Jun C, Lim S, et al. Multi-Imager Compatible, MR Safe, Remote Center
496 of Motion Needle-Guide Robot. *IEEE Trans Biomed Eng* 2018; 65(1):165–177.
- 497 31. Morikawa S, Haque H, naka S, et al. *An MR Image Navigation System for a Closed*
498 *Bore Scanner with a Needle Insertion Manipulator*. Paper presented at: ACCAS 2013
499 9th Asian Conference on Computer-Aided Surgery; 16–19 Sep. 2013.
- 500 32. Ewertsen C, Saftoiu A, Gruionu LG, Karstrup S, Nielsen MB. Real-time image fusion
501 involving diagnostic ultrasound. *AJR Am J Roentgenol* 2013; 200(3):W249–255.
- 502 33. Hakime A, Deschamps F, De Carvalho EG, Barah A, Auperin A, De Baere T.
503 Electromagnetic-tracked biopsy under ultrasound guidance: preliminary results.
504 *Cardiovas Intervent Radiol* 2012; 35(4):898–905.
- 505 34. Venkatesan AM, Kadoury S, Abi-Jaoudeh N, et al. Real-time FDG PET guidance during
506 biopsies and radiofrequency ablation using multimodality fusion with
507 electromagnetic navigation. *Radiology* 2011; 260(3):848–856.
- 508 35. Krucker J, Xu S, Venkatesan A, et al. Clinical utility of real-time fusion guidance for
509 biopsy and ablation. *J Vasc Interv Radiol* 2011; 22(4):515–524.
- 510 36. Bo XW, Xu HX, Wang D, et al. Fusion imaging of contrast-enhanced ultrasound and
511 contrast-enhanced CT or MRI before radiofrequency ablation for liver cancers. *Br J*
512 *Radiol* 2016; 89(1067):20160379.
- 513 37. Wang S-Y. Real-Time Fusion Imaging of Liver Ultrasound. *J Med Ultrasound* 2017;
514 25(1):9–11.
- 515 38. Krücker J, Xu S, Glossop N, et al. Electromagnetic tracking for thermal ablation and
516 biopsy guidance: clinical evaluation of spatial accuracy. *J Vasc Interv Radiol* 2007;
517 18(9):1141–1150.
- 518 39. Hakime A, Deschamps F, De Carvalho EG, Teriitehau C, Auperin A, De Baere T. Clinical
519 evaluation of spatial accuracy of a fusion imaging technique combining previously

- 520 acquired computed tomography and real-time ultrasound for imaging of liver
521 metastases. *Cardiovasc Intervent Radiol* 2011; 34(2):338–344.
- 522 40. Kurumi Y, Tani T, Naka S, et al. MR-guided microwave ablation for malignancies. *Int J*
523 *Clin Oncol* 2007; 12(2):85–93.
- 524